# A numerical model for the simulation of a solitary wave in a coastal region

F. Lasaponara & F. Camilli
*Department of Civil, Construction and Environmental Engineering,*
*Sapienza University of Rome, Italy*

## Abstract

In this paper we propose a numerical model for the simulation of tsunami wave propagation in a coastal region. The model can simulate the wave transformation due to refraction, shoaling, diffraction and breaking phenomena that take place in the surf zone and can simulate the wet front progress on the mainland. The above mentioned model is based on the numerical integration of the Fully Non-linear Boussinesq Equations in the deep water region and of the Non-linear Shallow Water Equations in the surf zone. These equations are expressed in an integral contravariant formulation and are integrated on a generalized curvilinear boundary conforming grid that can reproduce the complex morphology of the coastline. The numerical integration of the model equations is implemented by a high order Upwind WENO numerical scheme that involves an exact Riemann Solver. For the simulation of the wet front progress on the dry bed, the exact solution of the Riemann problem for the wet-dry front is used. The capacity of the proposed model to simulate the wet front progress velocity is tested by numerically reproducing the dam-break problem on a dry bed. The capacity of the proposed model to correctly simulate the tsunami wave evolution and propagation on the coastal region is tested by numerically reproducing a benchmark test case about tsunami wave propagation on a conic island.
*Keywords: coastal flooding, fully non-linear Boussinesq equations, non-linear shallow water equations, contravariant formulation, upwind WENO scheme, run up.*

## 1 Introduction

Coastal flooding risk is a potential source of huge social, economical and environmental costs. That is due to the fact that the major part of the global

population and of the biggest cities are placed in the coastal zone. In order to avoid enormous damage, caused by coastal flooding, it is essential to have the appropriate instruments to plan the whole coastal city system including coastal infrastructures and sea defences.

For the simulation of coastal flooding the modeling of the hydrodynamic phenomena which occur in coastal regions such as surface wave transformation, wave breaking and wave run up are of fundamental importance. Most of these phenomena can be represented by two dimensional fully non-linear Boussinesq equations (FNBE) that switches into the non-linear shallow water equations (NSWE) in the surf zone.

In coastal areas, slightly sloping and regular sea beds alternate with steep irregular bottoms and the coastlines can be characterized by articulated shapes and be interrupted by the presence of anthropic structures and/or river mouths. In order to simulate hydrodynamic phenomena over computational domains characterized by a complex boundary, two strategies can be followed. The first strategy is represented by the possibility of using unstructured grids (Hu and Shu [1], Gallerano and Napoli [2], Casonato and Gallerano [3], Cioffi *et al.* [4]). The second strategy is based on the numerical integration of the motion equations on a generalized curvilinear boundary conforming grid (Luo and Bewley [5], Gallerano and Cannata [6], Rossmanith *et al.* [7]). Classic forms of the Boussinesq equations include the lowest order of both frequency dispersion and non-linearities and are able to adequately represent wave phenomena only in a range of values of the water depth, $h_0$, to deep water wavelength, $L_0$, ratio up to 0.2. In order to overcome such restriction different formulations of Boussinesq equations have been proposed: Madsen and Sørensen [8], Nwogu [9], Wei *et al.* [10], Chen *et al.* [11]. Recently in literature integral forms (Gallerano *et al.* [12]) or new differential conservative forms of the Boussinesq equations (FNBE) expressed in terms of conserved variables (Erduran *et al.* [13], Tonelli and Petti [14], Roeber and Cheung [15], Shi *et al.* [16]) have been proposed. The above mentioned equations allows the simulation of breaking waves that can be represented by the discontinuities of the weak solution of the integral form of the NSWE, numerically solved by a shock capturing scheme (Toro [17], Brocchini and Dodd [18], Gallerano and Cannata [19], Gallerano *et al.* [20]). The above integral or differential conservative forms of the Boussinesq equations are able to simulate wave dynamics from deep water regions up to the coastline, do not need any additional term in order to take into account the wave breaking energy dissipation and do not require any empirical calibration. In order to apply a shock capturing method to Boussinesq equations expressed in differential conservative form, Roeber and Cheung [15] adopted the strategy proposed by Erduran *et al.* [13], consisting of using a hybrid finite volume-finite difference scheme.

In this paper an integral contravariant formulation of the motion equations is presented. These equations are solved by a hybrid finite volume–finite difference scheme: convective terms and terms related to the free surface elevation gradient are discretized by a high order finite volume upwind WENO scheme whereas

dispersive terms and the term related to the second order vertical vorticity are discretized by a finite-difference scheme.

The main goal of the present study is to provide a hydrodynamic model to reproduce and simulate all the phenomena that occur in coastal areas.

The paper is organized as follows: the integral contravariant formulation of the motion equations are presented in Section 2; the numerical scheme used to solve the equations is presented in Section 3; in Section 4 are shown benchmark tests case about a dam-break problem on a dry bed and the tsunami wave propagation on a conical island; conclusions are made in Section 5.

## 2  The motion equations

Let H = h + η be the total local water depth, where h is the local still water depth and η is the local surface displacement. The following vector can be defined as: $\vec{r} = H\vec{u_\alpha}$ and $\vec{s} = H\vec{u_2}$, in which $\vec{u_\alpha}$ is the horizontal velocity at an arbitrary distance from the still water level $z = \sigma$, $\vec{u_2}(z)$ consists of the second order terms in depth power expansion of the velocity vector and $\overline{\vec{u_2}}$ is the depth averaged value of $\vec{u_2}(z)$.

Considering the transformation $x^l = x^l(\xi^1 \xi^2)$ from the Cartesian coordinates $\vec{x}$ to the curvilinear coordinates $\vec{\xi}$ (note that hereinafter the superscript indicates the generic component and not the powers), $\vec{g}_{(l)} = \partial \vec{x}/\partial \xi^l$ is the covariant base vectors and $\vec{g}^{(l)} = \partial \xi^l/\partial \vec{x}$ is the contravariant base vectors. The metric tensor and its inverse are given respectively by $g_{lm} = \vec{g}_{(l)} \cdot \vec{g}_{(m)}$ and $g^{lm} = \vec{g}^{(l)} \cdot \vec{g}^{(m)}$. The Jacobian of the transformation is $\sqrt{g} = \sqrt{det(g_{lm})}$. The motion equations are integrated over an arbitrary surface element of area ΔA and are resolved in the direction $\lambda_k$

$$\lambda_k(\xi^1, \xi^2) = \vec{g}^{(l)}(\xi_0^1, \xi_0^2) \cdot \vec{g}_{(k)}(\xi^1, \xi^2) \tag{1}$$

We indicate $\vec{\tilde{g}}^{(l)} = \vec{g}^{(l)}(\xi_0^1, \xi_0^2)$ and $\vec{\tilde{g}}_{(k)} = \vec{g}_{(k)}(\xi^1, \xi^2)$. Then, according to Gallerano $et\ al.$ [12], the integral expressions of the FNBE in contravariant formulation is:

$$\iint_{\Delta A} \frac{\partial H}{\partial t} dA = - \int_L r^m n_m \, dL - \iint_{\Delta A} (s^l)_{,l} \, dA \tag{2}$$

$$\iint_{\Delta A} \vec{\tilde{g}}^{(l)} \cdot \vec{\tilde{g}}_{(k)} \frac{\partial r^{*k}}{\partial t} dA = - \int_L \left( \vec{\tilde{g}}^{(l)} \cdot \vec{\tilde{g}}_{(k)} \frac{r^k r^m}{H} + G \vec{\tilde{g}}^{(l)} \cdot \vec{g}^{(m)} \frac{H^2}{2} \right) n_m dL +$$

$$\iint_{\Delta A} \vec{\tilde{g}}^{(l)} \cdot \vec{\tilde{g}}_{(k)} GH g^{km} h_{,m} dA - \iint_{\Delta A} \vec{\tilde{g}}^{(l)} \cdot \vec{\tilde{g}}_{(k)} R^k dA -$$

$$\iint_{\Delta A} \vec{\tilde{g}}^{(l)} \cdot \vec{\tilde{g}}_{(k)} \frac{r^k}{H} (s^m)_{,m} dA + \iint_{\Delta A} \vec{\tilde{g}}^{(l)} \cdot \vec{\tilde{g}}_{(k)} \frac{\partial H}{\partial t} V'^k dA +$$

$$\iint_{\Delta A} \vec{\tilde{g}}^{(l)} \cdot \vec{\tilde{g}}_{(k)} HV''^k dA - \iint_{\Delta A} \vec{\tilde{g}}^{(l)} \cdot \vec{\tilde{g}}_{(k)} HT^k dA - \iint_{\Delta A} \vec{\tilde{g}}^{(l)} \cdot \vec{\tilde{g}}_{(k)} HW^k dA \tag{3}$$

which reduce to the NSWE by switching off dispersive terms. In the above equations, a comma with an index in a subscript stands for covariant differentiation, L is the contour line of the surface element of area ΔA and $n_m$ is the m-th component of the covariant outward normal, G is the constant of

gravity, $V^l = \frac{\partial V'^l}{\partial t} + V''^l$ and $T^l$ are the dispersive terms obtained by retaining terms up to $O(\mu^2)$ and $O(\varepsilon\mu^2)$ in depth power expansions of the horizontal velocity according to Wei et al. [10], $W^l$ is the term related to the approximation to the second order of the vertical component of the vorticity according to Chen et al.. [11] and $\vec{R}$ is the bottom resistance term. $r^{*l}$ is an auxiliary variable defined as: $r^{*l} = r^l + HV'^l$.

## 3   The numerical scheme

The numerical integration of eqns (2) and (3) is carried out by a high order upwind WENO scheme. The computational domain discretization is based on a grid defined by the coordinate lines $\xi^1$ and $\xi^2$ and by the points of coordinates $\xi^1 = i\Delta\xi^1$ and $\xi^2 = j\Delta\xi^2$, which represent the centres of the calculation cells $I_{i;j} = (\xi^1_{i-1/2}, \xi^1_{i+1/2}) \times (\xi^2_{i-1/2}, \xi^2_{i-1/2})$. $t^n$ is the time level of the known variables, while $t^{n+1} = t^n + \Delta t$ is the time level of the unknown variables. Let us indicate with $L(r^1, r^2)$ and with $L_B(s^1, s^2)$ respectively the first and the second term on the right-hand side of eqn (2). Let us indicate with $D(H, r^1, r^2)$ the sum of the convective and free surface elevation terms (which is split according to Xing and Shu [21] in order to ensure a well-balanced scheme) on the right-hand side of eqn (3) and with $D_B(H, r^1, r^2)$ the bottom friction term, the sum of dispersive terms and the term related to the approximation to the second order of the vertical vorticity on the right-hand side of this equation. By integrating eqns (2) and (3) over $[t^n, t^{n+1}]$ we get:

$$\widetilde{\widetilde{H}}_{i;j}^{(n+1)} = \widetilde{\widetilde{H}}_{i;j}^{(n)} - \frac{1}{\Delta A}\int_{t^n}^{t^{n+1}}[L(r^1, r^2) + L_B(s^1, s^2)]dt \tag{4}$$

$$\widetilde{r}^{*l(n+1)}_{i;j} = \widetilde{r}^{*l(n)}_{i;j} - \frac{1}{\Delta A}\int_{t^n}^{t^{n+1}}[D(H, r^1, r^2) + D_B(H, r^1, r^2)]dt \tag{5}$$

Eqns (4) and (5) represent the advancing from time level $t^n$ to time level $t^{n+1}$, of the variables $\widetilde{\widetilde{H}}_{i;j}$ and $\widetilde{r}^{*l}_{i;j}$. The state of the system is known at the centre of the calculation cell and it is defined by the cell-averaged values $\widetilde{\widetilde{H}}_{i;j}$ and $\widetilde{r}^{*l}_{i;j}$. In this paper, time integration of eqns (4) and (5) is carried out by means of a third order accurate Strong Stability Preserving Runge–Kutta method (SSPRK) reported in Spiteri and Ruuth [22]. The SSPRK method can be written in compact form as follows:

$$\widetilde{\widetilde{H}}_{i;j}^{(0)} = \widetilde{\widetilde{H}}_{i;j}^{(n)} \;;\quad \widetilde{r}^{*l(0)}_{i;j} = \widetilde{r}^{*l(n)}_{i;j} \tag{6}$$

$$\widetilde{\widetilde{H}}_{i;j}^{(p)} = \sum_{q=0}^{p-1}\left\{\Omega_{pq}H_{i,j}^{(q)} + \Delta t\varphi_{pq}\left[L\big(r^{1(q)}, r^{2(q)}\big) + L_B\big(s^{1(q)}, s^{2(q)}\big)\right]\right\} \tag{7}$$

$$\widetilde{r}^{*l(p)}_{i;j} = \sum_{q=0}^{p-1}\left\{\Omega_{pq}\widetilde{r}^{*l(p)}_{i;j} + \Delta t\varphi_{pq}\left[D\big(H^{(q)}, r^{1(q)}, r^{2(q)}\big) + \right.\right.$$
$$\left.\left. D_B\big(H^{(p)}, r^{1(p)}, r^{2(p)}, s^{1(p)}, s^{2(p)}\big)\right]\right\} \tag{8}$$

$$\widetilde{\widetilde{H}}_{i;j}^{(n+1)} = \widetilde{\widetilde{H}}_{i;j}^{(3)} \;\; ; \;\; \widetilde{\widetilde{r}}^{*\,l(n+1)}_{i;j} = \widetilde{\widetilde{r}}^{*\,l(3)}_{i;j} \tag{9}$$

where p=1;2;3. See Spiteri and Ruuth [22] for $\Omega_{pq}$ and $\varphi_{pq}$ values. The computation of $\boldsymbol{L}(r^1, r^2)$, $\boldsymbol{D}(H, r^1, r^2)$, $\boldsymbol{L_B}(s^1, s^2)$, $\boldsymbol{D_B}(H, r^1, r^2, s^1, s^2)$ terms needs the numerical approximation of the spatial integrals. According to the method proposed by Erduran *et al.* [13] and used among the others by Tonelli and Petti [14] and Shi *et al.* [16], this numerical approximation is carried out by means of a hybrid finite volume–finite difference scheme. By applying this method, once the values of the auxiliary variable $\widetilde{\widetilde{r}}^{*\,l}$ are known, the values of the original variable $\tilde{r}^l$ at each stage of the Runge–Kutta method are computed by solving the following equation:

$$\widetilde{\widetilde{r}}^{*\,l} = \tilde{r}^l + \widetilde{\widetilde{H}}\widetilde{\widetilde{V}}'^l \tag{10}$$

in which $\widetilde{\widetilde{V}}'^l$ includes first and second derivative of $\widetilde{\widetilde{r}}^{*\,l}/\widetilde{\widetilde{H}}$ with respect to $\xi^1$ and $\xi^2$ and cross derivatives. The numerical approximation of the derivatives in the $\widetilde{\widetilde{V}}'^l$ term is carried out by a second order central difference scheme.

Once the values of er are known, the $\boldsymbol{L_B}(s^1, s^2)$ and $\boldsymbol{D_B}(H, r^1, r^2, s^1, s^2)$ terms on the right-hand side of eqns (7) and (8) are discretized using a second order central difference scheme at the cell centroids, as in Wei and Kirby [10] and Shi *et al.* [16]. Since the $\boldsymbol{L_B}$ and $\boldsymbol{D_B}$ terms need to be updated using $H, r^1, r^2, s^1, s^2$ at the corresponding time step, an iteration is needed to achieve convergence, as suggested by Shi *et al.* [16]. Convective terms and terms related to the free surface elevation that define the $\boldsymbol{L}(r^1, r^2)$ and $\boldsymbol{D}(H, r^1, r^2)$ terms on the right-hand side of eqns (7) and (8) are computed by a high-order finite volume WENO scheme. According to the procedure proposed by Gallerano *et al.* [20] this numerical scheme is based on the following sequence:

1. Starting from cell averaged values, the point values of the unknown variables at the centre of the contour segments which define the calculation cells are computed by means of WENO reconstructions. Two WENO reconstructions defined on two adjacent cells are used to get two point values of the unknown variables at the centre of the contour segment which is common with the two adjacent cells.
2. The point values of the unknown variables at the centre of the contour segments are advanced in time by means of the so-called exact solution of a local Riemann problem, with initial data given by the pair of point-values computed by two WENO reconstructions defined on the two adjacent cells. In accordance with the procedure proposed by Rossmanith *et al.* [7], all necessary Riemann problems (Shock Waves for breaking and Rarefaction-Waves for wet-dry front) are solved in a locally valid orthonormal basis. This orthonormalization allows one to solve Cartesian Riemann problems that are devoid of geometric terms.
3. The spatial integrals that define the $\boldsymbol{L}(r^1, r^2)$ and $\boldsymbol{D}(H, r^1, r^2)$ terms are numerically approximated by means of a high order quadrature rule, starting from point values of the dependent variables computed at the previous step.

## 4   Results

### 4.1  The dam-break problem on a dry bed

In the typical dam-break problem a septum divides two regions: at the left of the septum still water of initial depth $h_0$ is present, while at the right of the septum the region is dry (Stoker [24]). The evolution of this initial condition upon removal of the septum, and so the suddenly release of the mound of water, is represented.

In this section the dam-break test is used to validate the adherence to the analytical solution of the solution obtained with the use of the model for the simulation of the wet and dry problem.

In the case in which a septum divides the wet and dry conditions and is suddenly removed at time $t = 0$, we have the typical Ritter solution (Stoker [24]) here shown in dimensionless form:

$$d^* = \frac{1}{9}\left(2 - \frac{x^*}{t^*}\right)^2 \tag{12}$$

$$u^* = \frac{2}{3}\left(\frac{x^*}{t^*} + 1\right) \tag{13}$$

The analytical solution for $h_0^* = 1$ is represented by solid line in fig. 1 at different dimensionless time $t^* = 0.006, 0.07, 0.12, 0.2$. In the same fig. 1, the numerical results, obtained by using the proposed wet and dry model, are in very good agreement with the analytical solution.
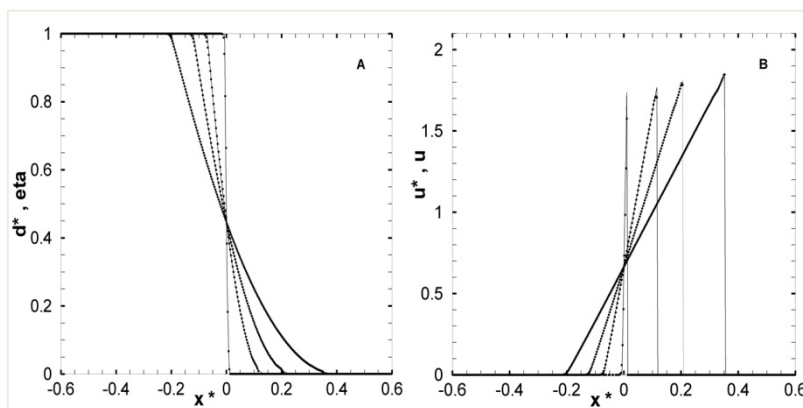


Figure 1:   The dam break problem on a dry bed. A) Water depth. B) Velocity. Points: numerical results. Solid line: analytical solution.

### 4.2  Solitary wave run-up on a conical island

In this section we simulate the run-up of a solitary wave onto a conical Island. To this aim we numerically reproduce a laboratory test of Liu *et al.* [25]. A definition sketch for the computational domain used for the simulation is shown in fig. 2.
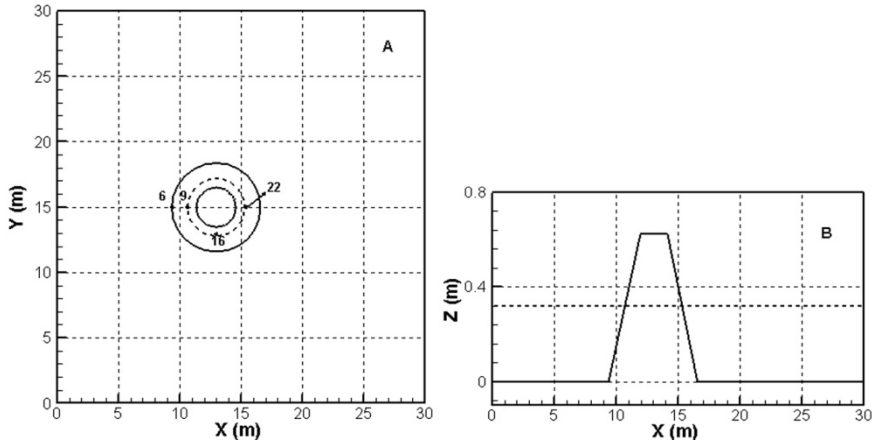
Figure 2:   Run-up of a solitary wave on a conical island. Schematic plot of the computational domain. A) Plane view. Outer circle: base of the island. Middle dashed circle: initial still water shoreline. Inner circle: island top. The dots represent measurement locations at 6:(9.4,15), 9:(10.4,15), 16:(13,12.42), 22:(15.6, 15). B) Cross section of the computational domain along the centreline (y=15 m). Dotted line: initial still water level.

The outer circle shows the base of the island, which is centred at (x,y)=(13, 15) m and has a radius R=3.6 m; the middle dashed circle represents the initial still water shoreline (radius R=2.32); the inner circle represents the island top (radius R=1.1 m); the island height is 0.625 m.

As initial condition a rightward propagating solitary wave is imposed to the left boundary of the domain, on an otherwise calm free surface. The following expressions (eqns (14) and (15)) are used for the free surface elevation $\eta$ and the depth averaged velocity component $u$ in the x direction:

$$\eta(t) = A sech^2 \left[ \sqrt{\frac{3A}{4h}} C(t - T) \right] \tag{14}$$

$$u(t) = \frac{C\eta(t)}{h+\eta(t)} \tag{15}$$

in which h is the still water depth, A is the amplitude of the incident wave, T is the time at which the wave crest enters the domain and $C = \sqrt{g(h + A)}$ is the wave celerity. In this work the test case C of Liu et al. [25] is reproduced: $h = 0.64\ m, A = 0.032\ m$ and $T = 2.45\ s$. The spatial discretization step is $dx = dy = 0.1\ m$, the time discretization step is $dt = 0.01\ s$.

In fig. 3 the comparison between the maximum computed run-up around the island and that measured by Liu et al. [25] is shown. The computed values of the maximum run-up around the island are in good agreement with the experimental
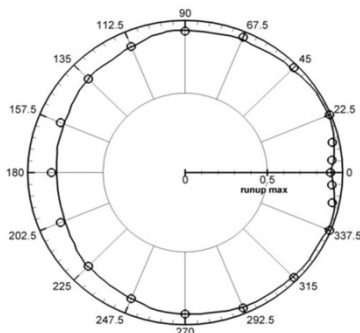
Figure 3:   Run-up of a solitary wave on a conical island. Maximum run-up around the conical island. Circles: measured data. Line: computed values.

data. It can be noted that the run-up on the back side of the island, caused by the collision of edge waves circling the island from both sides, is well simulated by the present model.

In fig. 4 the computed and measured time series from the measurement locations depicted in fig. 2 are shown. These four measurement locations have been chosen in order to represent the free surface elevation to the front, side, and rear of the island. From the comparison between the computed and measured values it can be seen that the proposed model is able to simulate the run-up at each measurement location around the island. Some secondary oscillation of the free surface elevation that has been observed during the laboratory experiments are slightly underestimated in the numerical simulation. The good agreement between the computed and observed values of the free surface elevation shows
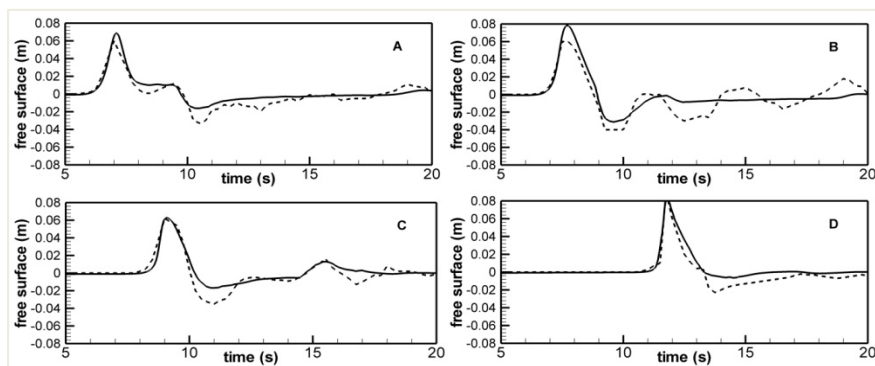


Figure 4:   Run-up of a solitary wave on a conical island. Time series from the measurement locations depicted in fig. 8: A) 6, B) 9, C) 16, D) 22. Full line: computed values. Dashed line: experimental data.

the ability of the proposed model to adequately simulate the large run-up heights produced by a tsunami wave on the lee side of small islands.

In fig. 5 a sequence of images that represents the evolution of a solitary wave on a conical island is shown. Fig. 5A) shows the simulation of the wave run-up on the forepart of the island. In the further frames (fig. 5B)–5C)) is possible to observe the perfect reproduction of the diffraction phenomena and, as a consequence, the wave run-up on the lateral beaches. The last frame (fig. 5D)) shows that in the back side of the island the surface elevation caused by the collision of the two waves front is maximum.
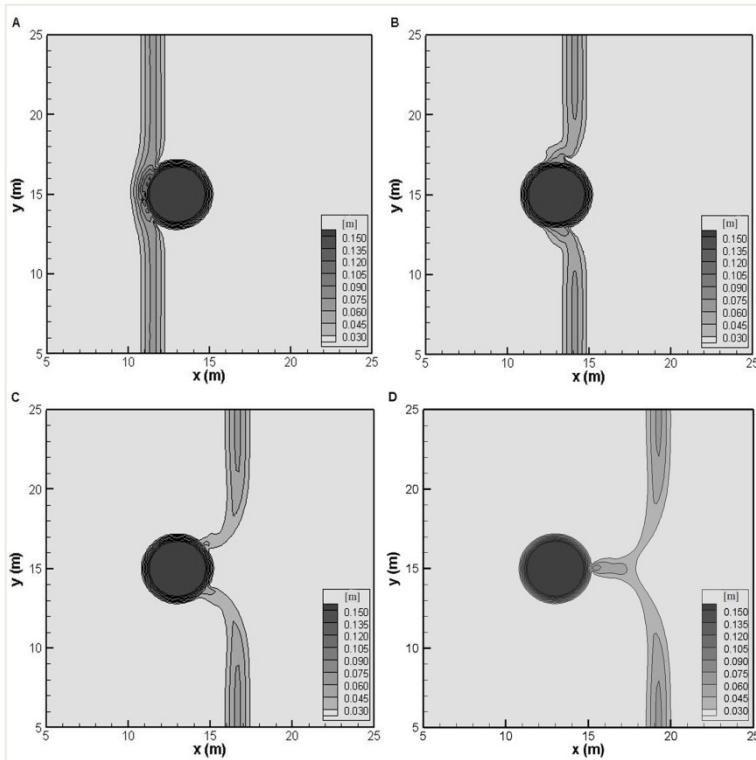


Figure 5:    Run-up of a solitary wave on a conical island.  Surface elevation contour levels at time A) t = 7.2 s, B) t = 9.7 s, C) t = 11.0 s, D) t = 12.2 s.

In fig. 6A) sequences of images that represent the evolution of a solitary wave with a height of 0.064 m on a planar slope of 1:30 with a rip channel excavated along the center line is shown.  From fig. 6 it is possible to observe how the solitary wave breaks before on the plane part of the beach (fig. 6B)) and then in the rip channel (fig. 6C)) where the wave maintain higher values of the height and of celerity caused by a deeper bed. As a consequence the wet-dry front arise the maximum height of run up in the rip channel before (fig. 6D)) and then in

the plane beach (fig. 6E)). The same happens for the run down (fig. 6E)–6F)). From fig. 6 is possible to highlight the capacity of this model to simulate the hydrodynamic swash zone phenomena on morphologically complex beach.
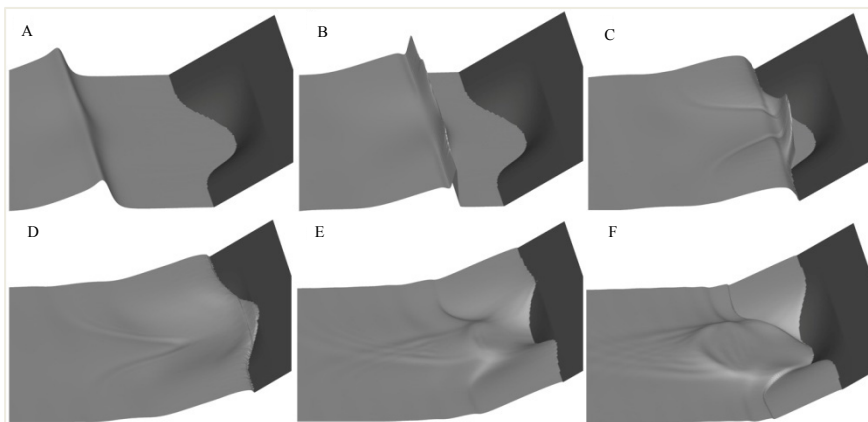


Figure 6:    Run-up of a solitary wave on a beach with a rip channel. Instantaneous surface elevation at different times.

## 5  Conclusion

In this paper a model based on a contravariant integral form of fully non-linear Boussinesq Equations (FNBE) has been tested. It had been also demonstrated that this model allows the simulation of wave propagation from deep water regions up to the coast line including the surf zone and wave transformation phenomena (refraction, diffraction, reflection, shoaling and breaking) in computational domains representing the complex morphology of real coastal regions.

Therefore this model could be a strong planning instrument to test tsunami wet front progress even in the presence of a complex coastal line, irregular seabed and the presence of marine infrastructures.

## References

[1]    Hu, C. & Shu, C.W., Weighted Essentially Non-oscillatory Schemes on Triangular Meshes, *J of Computational Physics*, **150(1)**, pp. 97-127, 1999.
[2]    Gallerano, F. & Napoli, E., A dynamic subgrid-scale tensorial Eddy viscosity model, *Continuum Mech. Thermo dyn,* **11(1)**, pp. 1-14, 1999.
[3]    Casonato, M., Gallerano, F., A finite difference self-adaptive mesh solution of flow in a sedimentation tank, *Int J for Num Meth in Fluids,* **10(6)**, pp. 697-711, 1990.

[4]  Cioffi, F., Gallerano, F. & Napoli, E., Three-dimensional numerical simulation of wind-driven flows in closed channels and basins, *J of Hydraulic Research*, **43(3)**, pp. 290-301, 2005.

[5]  Luo, H. & Bewley, T.R., On the contravariant form of the Navier–Stokes equations in time-dependent curvilinear coordinate systems, *J of Computational Physics*, **199**, pp. 355-375, 2004.

[6]  Gallerano, F. & Cannata, G., Compatibility of reservoir sediment flushing and river protection, *J of Hydraulic Engineering*, **137(10)**, pp. 1111-1125, 2011.

[7]  Rossmanith, J.A., Bale, D.S. & LeVeque, R.J., A wave propagation algorithm for hyperbolic systems on curved manifolds, *J of Computational Physics,* **199(2)**, pp. 631-662, 2004.

[8]  Madsen, P.A. & Sørensen, O.R., A new form of the Boussinesq equations with improved linear dispersion characteristics. Part 2. A slowly-varying bathymetry, *Coastal Engineering,* **18(3-4)**, pp. 183-204, 1992.

[9]  Nwogu, O., Alternative Form of Boussinesq Equations for Nearshore Wave Propagation, *J of Waterway, Port, Coastal, and Ocean Engineering,* **119(6)**, pp. 618-638, 1993.

[10]  Wei, G., Kirby, J.T., Grilli, S.T. & Subramanya, R., A fully non-linear Boussinesq model for surface waves. Part 1. Highly nonlinear unsteady waves, *J Fluid Mech,* **294**, pp. 71-92, 1995.

[11]  Chen, Q., Kirby, J.T., Dalrympe, R.A., Shi, F. & Thornton, E.B., Boussinesq modeling of longshore currents, *J of Geophysical Research,* **108(C11)**, pp. 3362, 2003.

[12]  Gallerano, F., Cannata, G. & Villani, M., An integral contravariant formulation of the fully non-linear Boussinesq equations, *Coastal Engineering,* **83**, pp. 119-136, 2014.

[13]  Erduran, K.S., Illic, S. & Kutija, V., Hybrid finite-volume finite-difference scheme for the solution of Boussinesq equations, *Int J for Num Meth in Fluids,* **49(11)**, pp. 1213-1232, 2005.

[14]  Tonelli, M. & Petti, M., Hybrid finite volume – finite difference scheme for 2DH improved Boussinesq equations, *Coastal Engineering,* **56(5-6)**, pp. 609-620, 2009.

[15]  Roeber, V. & Cheung, K.F., Boussinesq-type model for energetic breaking waves in fringing reef environments, *Coastal Engineering,* **70**, pp. 1-20, 2012.

[16]  Shi, F., Kirby, J.T., Harris, J.C., Geiman, J.D. & Grilli, S.T., A high-order adaptive time-stepping TVD solver for Boussinesq modeling of breaking waves and coastal inundation, *Coastal Engineering,* **43-44**, pp. 36-51, 2012.

[17]  Toro, E., *Shock-Capturing Methods for Free-Surface Shallow Flows,* John Wiley and Sons: Manchester, 2001.

[18]  Brocchini, M., Dodd, N., Nonlinear Shallow Water Equation Modeling for Coastal Engineering, *J Waterway, Port, Coastal, Ocean Eng,* **134(2)**, 104-120, 2008.

[19]  Gallerano, F. & Cannata, G., Central WENO scheme for the integral form of contravariant shallow-water equations, *Int J for Num Meth in Fluids,* **67(8)**, pp. 939-959, 2011.

[20]  Gallerano, F., Cannata, G. & Tamburrino, M., Upwind WENO scheme for Shallow Water Equations in contravariant formulation, *Computers & Fluids,* **62**, pp. 1-12, 2012.

[21]  Xing, Y., Shu, C.W., High order well-balanced finite volume WENO schemes and discontinuous Galerkin methods for a class of hyperbolic systems with source terms, *J of Computational Physics,* **214(2)**, pp. 567-598, 2006.

[22]  Spiteri, R.J. & Ruuth, S.J., A new class of optimal high-order strong-stability- preserving time discretization methods, *SIAM J Numer Anal,* **40(2)**, pp. 469-491.

[23]  Tonelli, M. & Petti, M., Shock-capturing Boussinesq model for irregular wave propagation, *Coastal Engineering,* 61, pp. 8-19, 2012.

[24]  Stoker, J. J., *Water Waves,* Interscience: New York, 1957.

[25]  Liu, X., Osher, S. & Chan, T., Weighted Essentially Non-oscillatory Schemes, *J of Computational Physics,* **115(1)**, pp. 200-212, 2002.